

# A kinematic model of a ducted flame

By A. P. DOWLING

Department of Engineering, University of Cambridge, Trumpington Street,  
Cambridge CB2 1PZ, UK

(Received 18 August 1998 and in revised form 22 March 1999)

A premixed ducted flame, burning in the wake of a bluff-body flame-holder, is considered. For such a flame, interaction between acoustic waves and unsteady combustion can lead to self-excited oscillations. The concept of a time-invariant turbulent flame speed is used to develop a kinematic model of the response of the flame to flow disturbances. Variations in the oncoming flow velocity at the flame-holder drive perturbations in the flame initiation surface and hence in the instantaneous rate of heat release. For linear fluctuations, the transfer function between heat release and velocity can be determined analytically from the model and is in good agreement with experiment across a wide frequency range. For nonlinear fluctuations, the model reproduces the flame surface distortions seen in schlieren films.

Coupling this kinematic flame model with an analysis of the acoustic waves generated in the duct by the unsteady combustion enables the time evolution of disturbances to be calculated. Self-excited oscillations occur above a critical fuel–air ratio. The frequency and amplitude of the resulting limit cycles are in satisfactory agreement with experiment. Flow reversal is predicted to occur during part of the limit-cycle oscillation and the flame then moves upstream of the flame-holder, just as in experimental visualizations. The main nonlinearity is identified in the rate of heat release, which essentially ‘saturates’ once the amplitude of the velocity fluctuation exceeds its mean. We show that, for this type of nonlinearity, describing function analysis can be used to give a good estimate of the limit-cycle frequency and amplitude from a quasi-nonlinear theory.

---

## 1. Introduction

In order to meet stringent emission requirements, combustors are increasingly being designed to operate in a premixed mode. Although this is beneficial as far as reducing  $\text{NO}_x$  is concerned, it has the disadvantage that premixed flames are particularly susceptible to self-excited oscillations and many premixed systems have experienced structural damage caused by combustion instability.

One of the simplest generic geometries is that of a confined premixed turbulent flame burning in the recirculation zone of a bluff body or rearward-facing step. Such configurations have been investigated extensively (see for example, Yamaguchi, Ohiwa & Hawegawa 1985; Sivasegaram & Whitelaw 1987; Schadow, Wilson & Gutmark 1988; Hedge, Reuter & Zinn 1988; Langhorne 1988; Sivasegaram, Thompson & Whitelaw 1989; Ahmed & Nejad 1992) and have been used as a model of the afterburner of an aeroengine. The ducted flame is unstable above a critical fuel–air ratio (Langhorne 1988) and linear disturbances grow into a periodic finite-amplitude limit cycle. These self-excited oscillations involve coupling between unsteady combustion and acoustic waves in the duct. Essentially, the velocity fluctuations associated

with acoustic waves in the duct perturb the flame and change the instantaneous rate of heat release. Since these fluctuations in heat release rate generate sound, the acoustic waves can gain energy from their interaction with the unsteady combustion (Rayleigh 1896). If this energy gain exceeds that lost on reflection at the ends of the duct, linear acoustic waves grow in amplitude until limited by nonlinear effects.

When predicting combustion oscillations it is crucially important to be able to describe the response of the rate of heat release to flow perturbations. Bloxsidge, Dowling & Langhorne (1988) investigated this experimentally by exciting a stable confined flame with weak harmonic sound waves. Their geometry consists of a circular duct in which the flame is stabilized in the wake of an axisymmetric centre-body. They found that the unsteady burning was determined principally by velocity fluctuations at the flame-holder, and gave an empirical form for the relationship between linear fluctuations in heat release rate and flow velocity. They expressed this relationship in an appropriate non-dimensional form and used it to develop a linear stability analysis for a flame burning in a duct. The Bloxsidge *et al.* theory predicts frequencies and mode shapes which are in good agreement with Langhorne's (1988) low-Mach-number experimental data. This theory was subsequently applied successfully to flows with higher inlet Mach numbers (Macquisten & Dowling 1993) and more complex geometries (Macquisten & Dowling 1995). The Bloxsidge *et al.* flame model has also been applied to other burner geometries with some success (Ohtsuka *et al.* 1998). But since this model is empirical, it is not able to explain how velocity fluctuations at the flame-holder cause unsteady burning. Flow visualizations show that, during unstable combustion, large-scale distortions occur in the flame front, which lead to time variations in the heat release rate (Smart, Jones & Jewel 1976; Pitz & Daily 1981; Keller *et al.* 1982; Smith & Zukoski 1985; Sterling & Zukoski 1987; Poinot *et al.* 1987; Yu, Trouvé & Daily 1991; Schadow & Gutmark 1992). Similar effects are seen in the numerical simulations of Kailasanath *et al.* (1991), Menon & Jou (1991), and Brookes, Cant & Dowling (1999).

Bloxsidge *et al.* (1998) give a complicated form for the transfer function between the perturbations in the rate of heat release and the flow velocity at the flame-holder. However, as noted by Dowling (1997), this expression is well approximated by a simple first-order lag law over the frequency range of the experimental data. Fleifil *et al.* (1996) have used the concept of a constant flame speed to investigate a premixed laminar flame in a duct, burning inwards from a ring on the duct wall. They find analytically that the heat release rate for linear disturbances is again related to the velocity fluctuation by a first-order lag law. In §2 we use the same approach to investigate a turbulent flame stabilized on a centre-body. For linear harmonic velocity fluctuations, the location of the flame surface can be calculated analytically. As in the calculations by Boyer & Quinard (1990), the flame becomes wrinkled with short-wavelength waves travelling along it. We find that a model in which the rate of heat release is related to the wrinkled flame surface area leads to a predicted transfer function in close agreement with the Bloxsidge empirical form. However, linear theory is not sufficient to investigate self-excited oscillations, since then the flow velocity and rate of heat release experience large changes in amplitude. Indeed flow reversal is observed during part of the oscillation cycle (Langhorne 1988), implying velocity perturbations exceed the mean. This is accompanied by large fluctuations in heat release rate, with burning almost extinguished at times (see for example Macquisten & Dowling 1993, figure 4). The kinematic flame model is extended to nonlinear oscillations in §2.2. Then the flame surface is predicted to undergo large-

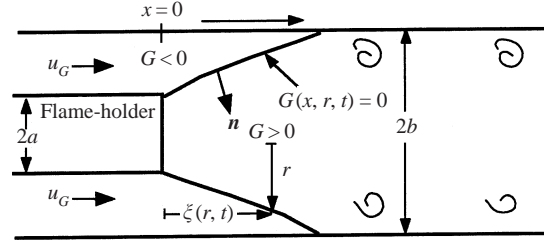


FIGURE 1. Geometry of the flame-holder and flame initiation surface.

scale distortions, which are reminiscent of the motion seen in schlieren films (Jones 1974) and still photographs (e.g. Smart *et al.* 1976). The flame model can be used to investigate the effect of this nonlinearity on the rate of combustion. It confirms the assumption made by Dowling (1997): whereas for weak perturbations the amplitude of the oscillations in heat release rate is proportional to that in the velocity at the flame-holder, for finite-amplitude oscillations, this relationship ‘saturates’ when the flow velocity reverses.

In §3, we use the kinematic flame model, together with the equations of conservation of mass, momentum and energy across the flame zone and the duct boundary conditions, to calculate self-excited oscillations of the flame. That is made tractable by recognizing as in Dowling (1997) that, while fluctuations in velocity and heat release are nonlinear, the fractional change in pressure remains small in this low-Mach-number flow. Therefore the acoustic waves are still linear, although nonlinear effects must be included in the relationship between the unsteady heat release rate and the flow velocity. This enables us to calculate the time evolution of the flow in a straightforward way. We find that self-excited oscillations occur above a critical fuel–air ratio. The characteristics of the resulting limit cycles are compared with Langhorne’s (1988) measurement. Describing function analysis is used in §4 to highlight the physical mechanisms that control the limit-cycle amplitude.

## 2. Development of the flame model

Consider a premixed flame with constant fuel–air ratio burning in a cylindrical duct, stabilized in the wake of an axisymmetric centre-body as shown in figure 1. Bloxsidge *et al.* (1988) investigated the relationship between flow perturbations and  $q(x, t)$ , the rate of heat release rate/unit duct length, for such a confined flame. They generated acoustic waves in the duct at a range of frequencies and measured the response of the flame to these imposed disturbances. The distribution of the rate of heat release was determined through measurements of the light emission from  $C_2$  radicals. Combustion was found to extend far downstream of the flame-holder and they observed that the fractional change in heat release rate/unit length at an axial position  $x$  was approximately equal to the change at the flame-holder at an earlier time. For fluctuations of frequency  $\omega$ , this statement implies

$$\frac{\hat{q}(x)}{\bar{q}(x)} = \frac{\hat{q}_G}{\bar{q}_G} e^{-i\omega\tau(x)}, \quad (2.1)$$

where the suffix  $G$  refers to flow conditions at  $x = 0$ , the location of the flame-holder or ‘gutter’. The overbar denotes a mean value, and the circumflex the complex amplitude of disturbances of frequency  $\omega$ , i.e.  $q(x, t) = \bar{q}(x) + \text{Re}(\hat{q}(x)e^{i\omega t})$ .

Bloxside *et al.* gave a specific form for the time delay  $\tau(x)$  and related  $q_G(t)$  to the particle velocity in the oncoming flow at the gutter  $u_G(t)$ . Although they give a complicated expression, as noted by Dowling (1997), in the frequency range of interest their flame model reduces to

$$\frac{\hat{q}_G}{\bar{q}_G} = \frac{1}{1 + i\omega\tau_1} \frac{\hat{u}_G}{\bar{u}_G}, \quad (2.2)$$

where

$$\tau_1 = 2\pi a/\bar{u}_G \quad (2.3)$$

and  $a$  is the radius of the centre-body. The empirical flame model described through (2.1)–(2.3) was initially derived from data on a stable flame, burning with low equivalence ratio  $\phi = 0.57$  in a low-Mach-number oncoming flow with  $\bar{M}_1 = 0.08$ . However, it has been demonstrated to describe the fluctuations in heat release rate in the self-excited oscillations that occur at higher fuel–air ratios (Bloxside *et al.* 1988). Experiments at a range of different flow conditions, including inlet velocities over four times faster than the initial tests (Macquisten & Dowling 1993), have confirmed the scaling of  $\tau_1$  on inlet velocity as in (2.3). Moreover, the flow impedance at the flame has been altered by changing the inlet geometry (see, for example, Macquisten & Dowling 1995) to check that the unsteady heat release does indeed depend on velocity fluctuations as in (2.2) and not on, say, pressure or density.

The flame model in (2.1)–(2.3) has been combined with the linearized equations of motion and used to predict the self-excited oscillations of a ducted flame. It leads to results for the susceptibility to instability and for the frequency of oscillation that have been validated against experimental data for a wide range of flow conditions (Bloxside *et al.* 1988; Macquisten & Dowling 1993, 1995). It has also been extrapolated to form the basis of a prediction scheme for low-frequency oscillations in the afterburners of aeroengines (Bloxside 1987) and currently used in industry. But, this flame model is, of course, entirely empirical, and has been deduced by simply expressing experimental results in an appropriate non-dimensional form. Fleifil *et al.* (1996) have derived a first-order lag law, similar in form to (2.2), for the unsteady rate of heat release in a laminar flame in a duct, burning inwards from a ring on the duct wall. We will extend their approach to a turbulent flame stabilized on a centre-body.

We assume that the flow is axisymmetric and that combustion begins on a surface whose axial position at radius  $r$  is given by  $x = \xi(r, t)$  as shown in figure 1. The flame initiation surface is therefore described by  $G(x, r, t) = 0$ , where

$$G(x, r, t) = x - \xi(r, t). \quad (2.4)$$

This surface is assumed to propagate normal to itself at constant speed  $S_u$  relative to the unburnt fluid, i.e. the surface  $G = 0$  moves in the direction of its normal  $\mathbf{n}$  with speed  $\mathbf{u} \cdot \mathbf{n} - S_u$ , where  $\mathbf{u} = (u, v)$  is the unburnt fluid particle velocity and  $\mathbf{n}$  points downstream as shown in figure 1. Mathematically this statement is equivalent to  $\tilde{D}G/Dt = 0$ , where  $\tilde{D}/Dt$  denotes a convected derivative with velocity  $\mathbf{u} - S_u\mathbf{n}$ :

$$\frac{\tilde{D}G}{Dt} = \frac{\partial G}{\partial t} + (\mathbf{u} - S_u\mathbf{n}) \cdot \nabla G = 0. \quad (2.5)$$

After rewriting  $\mathbf{n} = \nabla G/|\nabla G|$ , we obtain the familiar G-equation (Markstein 1964; Kerstein, Ashurst & Williams 1988)

$$\frac{\partial G}{\partial t} + \mathbf{u} \cdot \nabla G = S_u|\nabla G|. \quad (2.6)$$

Substitution for  $G$  from (2.4) gives

$$-\frac{\partial \xi}{\partial t} + u - v \frac{\partial \xi}{\partial r} = S_u \left( 1 + \left( \frac{\partial \xi}{\partial r} \right)^2 \right)^{1/2}. \quad (2.7)$$

An equation of this sort for the location of a flame surface has been used extensively (see for example Subbaiah 1983; Yang & Culick 1986; and Poinso & Candel 1988) and generally requires a numerical solution. The simplification made by Fleifil *et al.* was to assume the density change across the flame front to be negligible. Then an analytical solution can be derived. We make the same assumption but for different reasons. For the laminar flame, Fleifil *et al.* consider the fuel–air ratio to be so low that the overall expansion is negligible. That is not the case for the turbulent flame, but then the combustion zone is extensive. Bloxside *et al.* detected combustion continuing at 30 duct radii downstream of the flame-holder, with  $q_G(t)$  the heat release rate/duct length near the flame-holder being very small. This suggests that, for the turbulent flame, we should view the surface  $G(x, r, t) = 0$  as an initiation front, with negligible density change across it. Combustion continues downstream of this surface in turbulent flamelets, where fluctuations in heat release lag perturbations at the initiation surface according to the Bloxside *et al.* form in equation (2.1).

The Bloxside empirical form in (2.2) provides further evidence that the overall density change does not influence the flame dynamics in this initiation region. It describes a universal function relating fractional changes in the heat release rate  $q_G(t)$  and oncoming flow velocity  $u_G(t)$ , that is independent of fuel–air ratio and hence of density ratio.

When the density change across the surface  $G(x, r, t) = 0$  is negligible, the particle velocity in (2.7) is given by that in the oncoming flow ( $u_G, 0$ ). Equation (2.7) then simplifies:

$$\frac{\partial \xi}{\partial t} = u_G - S_u \left( 1 + \left( \frac{\partial \xi}{\partial r} \right)^2 \right)^{1/2}. \quad (2.8)$$

In this section we derive a kinematic model of the unsteady heat release. This involves solving (2.8) to determine the flame location  $\xi(r, t)$  for a specified oncoming velocity, which for simplicity we will assume to be independent of radius,  $u_G(t)$ . Once  $\xi(r, t)$  is known, the instantaneous flame surface area  $A(t)$  can be readily calculated, since

$$A(t) = \int_a^b 2\pi r \left( 1 + \left( \frac{\partial \xi}{\partial r} \right)^2 \right)^{1/2} dr, \quad (2.9)$$

where  $b$  is the duct radius. We will take the rate of heat release in the flame spreading region to be proportional to this instantaneous flame area, i.e.

$$q_G(t) \propto A(t). \quad (2.10)$$

### 2.1. Linear fluctuations

For linear perturbations of frequency  $\omega$ , we can solve for the flame surface analytically. Consider an imposed velocity fluctuation of the form,  $u_G(t) = \bar{u}_G + \text{Re}(\hat{u}_G e^{i\omega t})$ . We express the resulting flame surface oscillation in the form  $\xi(r, t) = \bar{\xi}(r) + \text{Re}(\hat{\xi}(r) e^{i\omega t})$ . Since the flame is attached at the flame-holder,

$$\xi(a, t) = 0, \quad \text{i.e.} \quad \bar{\xi}(a) = \hat{\xi}(a) = 0. \quad (2.11)$$

The mean value of equation (2.8) leads directly to  $\bar{u}_G = S_u(1 + (d\bar{\xi}/dr)^2)^{1/2}$  which, after integration and application of the boundary condition (2.11), gives a conical surface for the mean position of the flame front:

$$\bar{\xi}(r) = (r - a)(\bar{u}_G^2 - S_u^2)^{1/2}/S_u. \quad (2.12)$$

Linearization in the amplitude of the perturbation reduces (2.8) to a first-order ODE for  $\hat{\xi}(r)$ :

$$\begin{aligned} i\omega \hat{\xi} &= \hat{u}_G - S_u \frac{d\hat{\xi}}{dr} \frac{d\bar{\xi}}{dr} \left( 1 + \left( \frac{d\bar{\xi}}{dr} \right)^2 \right)^{-1/2} \\ &= \hat{u}_G - \frac{d\hat{\xi}}{dr} \frac{S_u}{\bar{u}_G} (\bar{u}_G^2 - S_u^2)^{1/2}, \end{aligned} \quad (2.13)$$

after substitution for  $\bar{\xi}(r)$  from (2.12). Use of an integrating factor makes the solution of this ODE for  $\hat{\xi}(r)$  straightforward, and application of the boundary condition (2.11) leads to

$$\hat{\xi}(r) = \frac{\hat{u}_G}{i\omega} (1 - \exp(-i\omega(r - a)/S_u(1 - S_u^2/\bar{u}_G^2)^{1/2})). \quad (2.14)$$

Any unsteadiness in the oncoming velocity  $u_G(t)$  forces perturbations to the flame front which propagate radially outwards from the flame-holder.

The flame area can be calculated by substitution for  $\xi(r, t)$  from (2.12) and (2.14) into (2.9) and integration across the duct. Its mean and complex amplitude are described by

$$\bar{A} = \pi(b^2 - a^2)\bar{u}_G/S_u \quad (2.15a)$$

and

$$\hat{A} = \hat{u}_G \frac{2\pi(b - a)}{i\Omega S_u} \left( a - b e^{-i\Omega} + \frac{b - a}{i\Omega} (1 - e^{-i\Omega}) \right), \quad (2.15b)$$

where the non-dimensional frequency  $\Omega$  is given by

$$\Omega = \omega(b - a)/S_u(1 - S_u^2/\bar{u}_G^2)^{1/2}. \quad (2.16)$$

Finally it follows from (2.10) that

$$\frac{\hat{q}_G}{\bar{q}_G} = \frac{\hat{A}}{\bar{A}} = \frac{\hat{u}_G}{\bar{u}_G} f(\Omega), \quad (2.17)$$

where

$$f(\Omega) = \frac{2}{i\Omega(a + b)} \left( a - b e^{-i\Omega} + \frac{b - a}{i\Omega} (1 - e^{-i\Omega}) \right). \quad (2.18)$$

This kinematic flame model leads to heat release fluctuations that are proportional to the velocity perturbations in the incoming flow, the constant of proportionality  $f(\Omega)$  being a function of frequency, just as in the Bloxsidge *et al.* empirical form.

For small values  $\Omega$ , the exponentials in (2.18) can be expanded as a power series. After some algebra this leads to

$$f(\Omega) \approx \frac{1}{1 + i\omega\tau_1 + (i\omega)^2\tau_1\tau_3}, \quad (2.19)$$

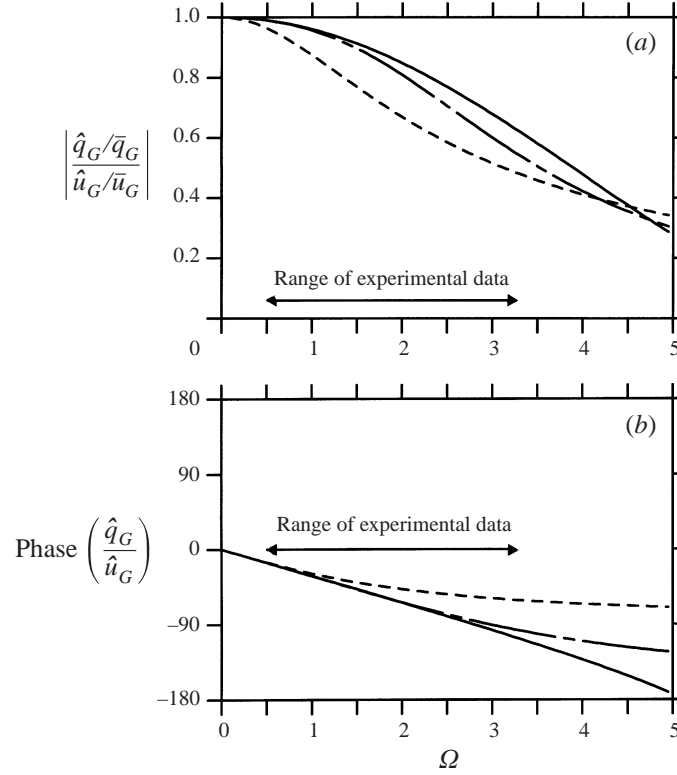


FIGURE 2. Transfer function between rate of heat release  $q_G(t)$  and the velocity  $u_G(t)$  as a function of non-dimensional frequency  $\Omega = \omega(b-a)/S_u(1 - S_u^2/\bar{u}_G^2)^{1/2}$ , for  $b = 2a$ : —, linearized flame model of (2.17)–(2.18); -·-·-, first-order lag law, empirical form of Bloxsidge *et al.* (1988); - - - -, second-order lag law, empirical form of Dowling (1997).

where

$$\tau_1 = \frac{(2b+a)(b-a)}{3(b+a)S_u(1 - S_u^2/\bar{u}_G^2)^{1/2}} \quad \text{and} \quad \tau_3 = \tau_1 \frac{7b^2 + 4ab + a^2}{4(2b+a)^2}. \quad (2.20)$$

For small  $\omega\tau_1$ , equation (2.19) reduces to the first-order lag law of Bloxsidge *et al.* The higher-frequency correction leads to a second-order lag equation as deduced from empirical considerations by Dowling (1997). The form predicted in (2.17) for the heat release rate is compared with that derived from experimental data in figure 2. There is one parameter to be specified in this flame model: the ratio of flame speed  $S_u$  to oncoming mean velocity  $\bar{u}_G$ . The turbulent flame speed is not known for the Bloxsidge *et al.* experiment. Instead we have chosen  $S_u$  so that  $\tau_1$  in (2.20) agrees with the Bloxsidge form in (2.3) for their geometry ( $b = 2a$ ). This leads to  $S_u = 0.09\bar{u}_G$ . The data are based on burning ethylene in an oncoming flow with  $\bar{u}_G = 37 \text{ m s}^{-1}$ . For such a flow, the ratio  $S_u/\bar{u}_G = 0.09$  corresponds to a flame speed  $S_u = 3.6 \text{ m s}^{-1}$ . This is about ten times faster than the laminar flame speed for an equivalence ratio of 0.7 (Abu-Orf & Cant 1996), a reasonable value for a turbulent flame (Catlin, Fairweather & Ibrahim 1995). It is clear from figure 2 that there is good agreement between this kinematic flame model and experiment. The magnitude and phase of the transfer function between heat release and velocity are well matched throughout the range of the experimental data,  $0.5 \leq \Omega \leq 3.2$ .

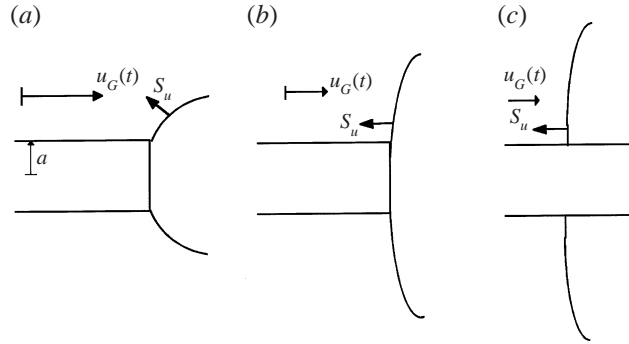


FIGURE 3. The boundary condition on  $r = a$ , (a)  $u_G(t) > S_u$ ,  $\xi(a, t) = 0$ ,  $\partial\xi/\partial r$  given by (2.21); (b)  $u_G(t) = S_u$ ,  $\partial\xi/\partial r = 0$ ; (c)  $u_G(t) < S_u$  or  $\xi(a, t) < 0$ ,  $\partial\xi/\partial r = 0$ .

The kinematic flame model, defined through equations (2.16)–(2.18) and (2.1), can be used instead of the Bloxsidge *et al.* empirical form in (2.2) in a linear stability analysis of a ducted flame. But it is evident from figure 2 that the expressions (2.2) and (2.17) are so similar that this will not lead to significantly different results from those presented in Bloxsidge *et al.* (1988) and Macquisten & Dowling (1993). It does, however, provide a physical basis for the empirical form.

Equations (2.16) and (2.17) display the important cross-stream length explicitly. It is  $b - a$ , the distance the flame has to spread between the lip of the flame-holder and the duct wall, that influences the flame-holder, not the flame-holder width as implied in the Bloxsidge form in (2.3). This has been used when extending the flame model from a single centre-body to the more complicated geometry of an aeroengine after-burner with several flame-holders.

For linearized fluctuations then, this kinematic flame model provides a physical interpretation of an empirical form given by Bloxsidge *et al.* It also shows how that form should be changed for burners of different geometries. However, its main advantage is that it can be extended to describe nonlinear flame motion.

## 2.2. Nonlinear fluctuations

The perturbations that occur in the self-excited oscillations of a ducted flame are sufficiently intense that the flow reverses during part of the cycle and the flame front moves upstream of the flame holder (Langhorne 1988). Then the fluctuations in velocity  $u'_G(t)$  are of the same order as the mean and the linearization of §2.1 is no longer appropriate. The kinematic flame model can be readily extended to describe flame motion in an oncoming flow in which  $u_G(t)$  varies significantly. It is then necessary to solve the PDE in (2.8) numerically and careful consideration must be given to the appropriate choice of boundary condition.

For linear fluctuations, we assumed that the flame was attached at the flame-holder, i.e. that  $\xi(a, t) = 0$  (see (2.11)). When this condition is applied, equation (2.8) can be rearranged to give

$$S_u \frac{\partial \xi}{\partial r} = (u_G^2(t) - S_u^2)^{1/2} \quad \text{on } r = a, \quad (2.21)$$

as shown in figure 3(a). This only has a solution when  $u_G(t) > S_u$ . For  $u_G(t) < S_u$  it is no longer possible for the flame to remain attached at the flame-holder with  $\xi(a, t) = 0$ . We then need to apply a different boundary condition on  $r = a$ . For  $u_G(t) = S_u$ ,  $\partial\xi/\partial r = 0$  on  $r = a$  and the flame-front leaves the flame-holder normally

as shown in figure 3(b). When  $u_G(t)$  drops below  $S_u$ , the flame leaves the flame-holder and propagates upstream as in figure 3(c). We insist that the flame front at  $r = a$  remains perpendicular to the centre-body all the time it is detached from the end of the flame-holder. This imposed boundary condition is physically reasonable. In a case with density differences across the flame front, it is the only boundary condition that meets the requirements of zero normal velocity on the sidewalls of the flame-holder, both upstream and downstream of the flame front. This leads to a boundary condition with some hysteresis:

on  $r = a$

$$\left. \begin{aligned} S_u \frac{\partial \xi}{\partial r} &= (u_G^2(t) - S_u^2)^{1/2} \quad \text{for } u_G(t) \geq S_u \quad \text{and} \quad \xi(a, t) = 0, \\ \frac{\partial \xi}{\partial r} &= 0 \quad \text{if } u_G(t) \leq S_u \quad \text{or} \quad \xi(a, t) < 0. \end{aligned} \right\} \quad (2.22)$$

For specified forcing  $u_G(t)$ , equation (2.8) can be integrated in time to determine the evolution of the flame-front.

As an illustrative example, we have perturbed a flame, initially in its equilibrium position  $\bar{\xi}(r) = (r - a)(\bar{u}_G^2 - S_u^2)^{1/2}/S_u$ , by an unsteady inlet flow  $u_G(t) = \bar{u}_G(1 + VH(t) \sin \omega t)$ . The results in figure 4 are for  $V = 1.15$ ,  $b = 4a$ ,  $\Omega = 2$  and  $S_u = 0.09\bar{u}_G$ . The flame surface rapidly settles into a periodic oscillation and various phases are shown in figure 4. In this plotted sequence, the flow velocity  $u_G(t)$  starts from its mean value in figure 4(a) and then decreases. Once the instantaneous flow velocity drops below the flame speed as in (c) the flame begins to move upstream of the flame-holder. When the flow velocity again exceeds the flame speed, (f), the flame propagates downstream but there is a convection time delay before it reattaches. This is seen clearly by a comparison of (b) and (f): the flow velocities are equal at these times, but the flame has quite different forms. The flame boundary conditions in (2.22) exhibit hysteresis. By (g) the flame has reattached to the flame-holder. Reattachment leads to an abrupt change in the slope of the flame surface or 'necking', which subsequently convects downstream. As the oncoming velocity reduces again, the flame front first propagates outwards towards the duct walls (compare (l) and (b)) before travelling upstream of the flame-holder. The cycle then repeats. Many of the features of this predicted flame distortion are seen in schlieren films (Jones 1974) and photographs (Smart *et al.* 1976) of perturbed flames. In particular, the experiments clearly show propagation of the flame upstream of the flame-holder. In a similar way, flame reattachment leads to an abrupt change in the slope of the flame surface, which is then convected downstream. The propagation of the flame towards the duct walls (as in (a)–(c)) is also evident as a precursor to flame detachment.

We are particularly interested in the flame surface area because, according to our model, this is directly related to the rate of heat release. Once  $\xi(r, t)$  has been determined, the flame area can be obtained from (2.9) by numerical integration. Results for different values of the non-dimensional forcing amplitude are shown in figure 5. Predictions given in (2.15) from the linearized theory are also shown for comparison. At low non-dimensional frequencies, the flame area and inlet velocity are in phase. At higher frequencies, the instantaneous flame area lags the velocity in agreement with (2.15)–(2.20). Nonlinearity is of a simple form. Indeed for  $V \leq 1$ , the instantaneous flame area is well predicted by the linearized solution in §2.1. For  $V \geq 1$ , linear theory unphysically predicts a negative flame area during part of the cycle. In practice, the minimum possible flame area is when the flame is straight across the duct and is equal to  $\pi(b^2 - a^2)$ . We see from figure 5(a) that this is achieved

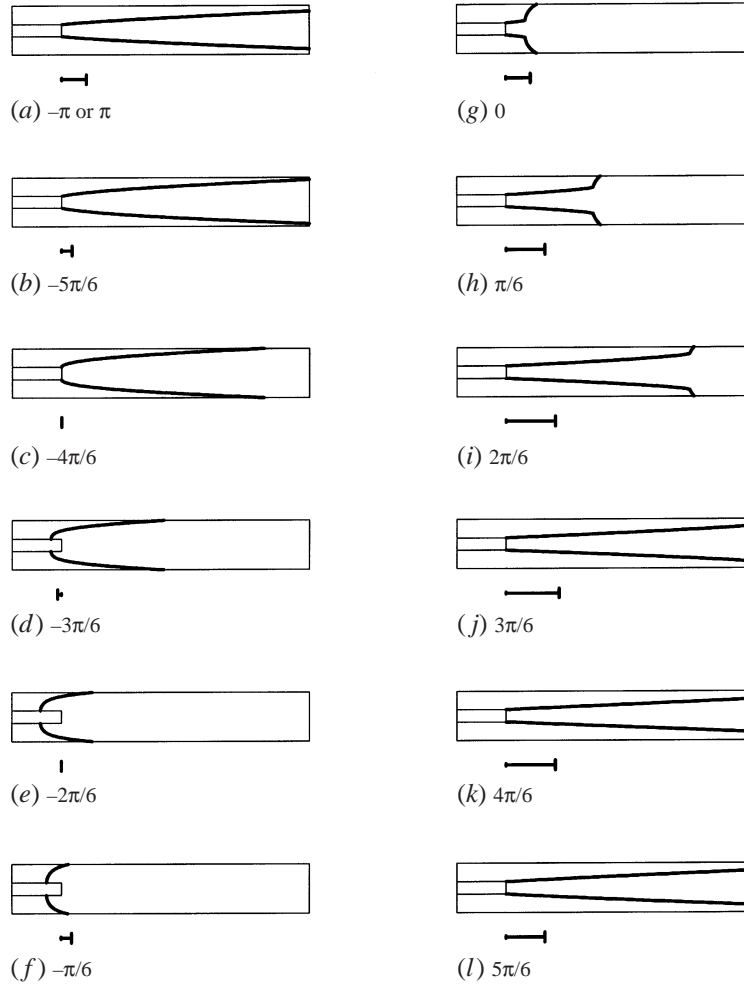


FIGURE 4. Periodic fluctuations in the position of the flame surface for the unsteady inlet flow  $u_G(t) = \bar{u}_G(1 + VH(t) \sin \omega t)$ ,  $V = 1.15$ ,  $b = 4a$ ,  $\Omega = 2$  and  $S_u = 0.09\bar{u}_G$ . The value of  $\omega t - 2\pi N$  increases from  $-\pi$  to  $\pi$  in steps of  $\pi/6$ ;  $\dashv$  denotes the instantaneous velocity  $u_G(t)$ .

at low frequencies. At higher frequencies, the flame front remains curved resulting in a larger minimum flame area (see figures 5(b) and 5(c)).

Once the flame area  $A(t)$  is known, the rate of heat released within the duct follows from combining (2.1) and (2.10)

$$\frac{q(x, t)}{\bar{q}(x)} = \frac{q_G(t - \tau(x))}{\bar{q}_G} = \frac{A(t - \tau(x))}{\bar{A}}. \quad (2.23)$$

We have developed a kinematic flame model which describes how fluctuations in the velocity at the flame-holder lead to unsteadiness in the rate of heat release. However, fluctuations in heat release generate acoustic waves which in turn cause upstream velocity fluctuations. There is then the possibility of self-excited oscillations, which are considered in § 3.

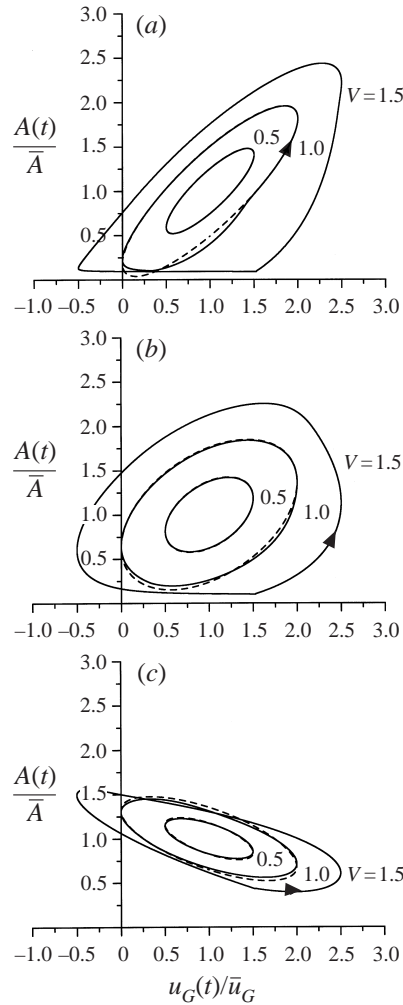


FIGURE 5. Phase-space plots of flame area  $A(t)$  for  $u_G(t) = \bar{u}_G(1 + VH(t) \sin \omega t)$ ,  $b = 2a$ ,  $S_u = 0.09\bar{u}_G$ ; —, nonlinear flame model; - - - - -, linearized form in equation (2.15). (a)  $\Omega = 1$ , (b)  $\Omega = 2$ , (c)  $\Omega = 4$ .

### 3. Nonlinear self-excited oscillations of a ducted flame

In this section we first investigate the acoustic waves generated in a duct by unsteady combustion. These are then combined with the flame model of §2 to predict self-excited oscillations. For definiteness we will consider the geometry shown schematically in figure 6: the flow at the inlet to the working section is choked and the duct exit is open. This corresponds to Langhorne's experiment (Langhorne 1988), where above a critical fuel-air ratio the flame is observed to undergo periodic self-excited oscillations. Linear theories for these self-excited oscillations are well established (see for example Bloxsidge *et al.* 1988; Macquisten & Dowling 1993). They give satisfactory predictions for the susceptibility to instability and for the frequencies of oscillation. The linearized flame model of §2.1 could be incorporated into these linearized theories. However, for the Langhorne geometry, the kinematic flame model leads to flame transfer functions which are so similar to the empirical

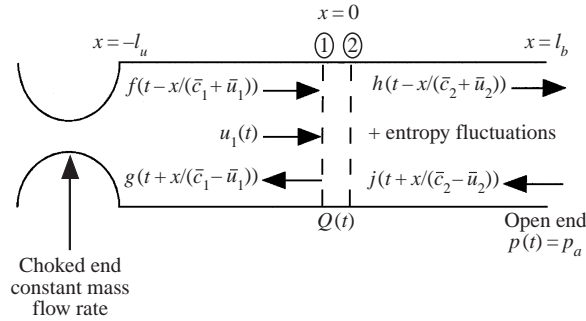


FIGURE 6. Schematic diagram of the duct geometry and flow.

form used previously in the linear theory (see figure 2 for the comparison) that this will not lead to significantly new results. At an unstable operation condition, linear theory predicts disturbances which grow exponentially with time. In this section, we will investigate whether the nonlinear flame model of §2.2 leads to finite-amplitude limit cycles representative of those observed experimentally.

The frequencies of interest are low, with acoustic wavelengths very long in comparison with the duct diameter. Therefore only plane acoustic waves carry energy and higher-order modes decay exponentially fast with axial distance. In practice, combustion is distributed along the duct downstream of the flame-holder. However, since our interest is in focusing on nonlinear effects, we will simplify the heat input by considering it concentrated over a short axial length. We enclose this burning region by a control surface, whose axial length may extend several duct diameters but is short in comparison with the acoustic wavelength. While the flame geometry and hence the flow within the control volume are two-dimensional as described in §2, the acoustic waves outside the control surface revert to being one-dimensional and couple to the heat release rate integrated throughout the control volume. Considering the heat release as concentrated in this way and neglecting the rate of change of mass, momentum and energy of the fluid within the small control volume may lead to some inaccuracy in the predicted frequency (Dowling 1995), but it makes the analysis sufficiently tractable to clarify the role of nonlinearities.

The nonlinear form for the instantaneous total rate of heat release follows from (2.23). We will take it to be given by

$$\frac{Q(t)}{Q} = \frac{A(t - \bar{\tau})}{A}. \quad (3.1)$$

$\bar{\tau}$  represents an average time delay which, to be consistent with the empirical form for  $Q(t)$  in Dowling (1997), we will assume to be equal to  $0.4l_b/\bar{u}_1$ , where  $l_b$  is the length of duct downstream of the flame-holder and  $\bar{u}_1$  is the mean velocity upstream of the flame-holder.  $A(t)$  is to be solved by integration of (2.8) with the boundary conditions (2.22) once  $u_G(t)$  is known.

A common approach when considering nonlinear combustion oscillations is to expand the flow disturbances as a Galerkin series (Lores & Zinn 1973; Awad & Culick 1986; Culick 1988, 1994; Margolis 1993; and Wicker, Yoon & Yang 1995). But instead, we follow the wave-based method of Dowling (1997). This has the advantage that, after application of the duct boundary conditions, only two time-varying wave strengths are required to resolve all the plane wave modes of the duct/flame arrangement. In contrast, an infinite number of time-varying coefficients

must be determined to obtain this level of resolution from a Galerkin series. The formulation of the equations for the acoustic waves is the same as in Dowling (1997), but we will repeat the main steps here for completeness. First we combine the equations of conservation of mass, momentum and energy flow rates across the flame zone,  $x = 0$ , with the perfect gas equation, to lead to two equations which are independent of the density and temperature downstream of the burning region. The momentum equation can be written in the form

$$[p]_1^2 + \rho_1 u_1 [u_1]_1^2 = 0, \quad (3.2)$$

where  $p$  is the pressure and  $\rho$  the density. The suffices 1 and 2 denote flow quantities just upstream of the flame-holder and downstream of the burning region respectively. We have neglected any drag on the fluid exerted by the flame-holder, which has previously been shown only to have a small effect (Dowling 1995, §4). Use of the perfect gas equation  $T\rho = p/R$  enables the energy equation to be written in the form

$$\frac{\gamma}{\gamma - 1} [pu]_1^2 + \rho_1 u_1 \left[ \frac{1}{2} u^2 \right] = \frac{Q}{\pi b^2}, \quad (3.3)$$

where  $\gamma$  is the ratio of specific heat capacities.

In acoustic waves,  $p' \sim O(u'\bar{\rho}\bar{c})$ , where  $\bar{c}$  is the speed of sound. Hence

$$\frac{p'}{\bar{p}} = O(\gamma\bar{M}) \frac{u'}{\bar{u}}, \quad (3.4)$$

where  $\bar{M}$  is the mean Mach number. For the low-Mach-number flows in which the flame will burn, the fractional pressure fluctuation remains small, even when  $u'/\bar{u} \sim O(1)$ . Since  $u'$  is also much less than  $\bar{c}$ , the acoustic waves can be treated as linear. Therefore, for the region upstream of the combustion zone,  $-l_u \leq x \leq 0$ , we can write the flow variables in the form

$$p(x, t) = \bar{p}_1 + f \left( t - \frac{x}{\bar{c}_1 + \bar{u}_1} \right) + g \left( t + \frac{x}{\bar{c}_1 - \bar{u}_1} \right), \quad (3.5a)$$

$$u(x, t) = \bar{u}_1 + \frac{1}{\bar{\rho}_1 \bar{c}_1} \left( f \left( t - \frac{x}{\bar{c}_1 + \bar{u}_1} \right) - g \left( t + \frac{x}{\bar{c}_1 - \bar{u}_1} \right) \right), \quad (3.5b)$$

with

$$\rho(x, t) = \bar{\rho}_1 + \frac{1}{\bar{c}_1^2} \left( f \left( t - \frac{x}{\bar{c}_1 + \bar{u}_1} \right) + g \left( t + \frac{x}{\bar{c}_1 - \bar{u}_1} \right) \right); \quad (3.5c)$$

$f$  and  $g$  denote the strength of the downstream- and upstream-propagating acoustic waves respectively.

As in Langhorne's (1988) experiments, we consider the inlet flow at  $x = -l_u$  to be choked. The mass flow rate there is then constant leading to a simple description of how an incoming wave is reflected:

$$f(t) = \frac{1 - \bar{M}_1}{1 + \bar{M}_1} g(t - \tau_u), \quad (3.6)$$

where  $\bar{M}_1$  is the mean Mach number upstream of the burning zone and  $\tau_u = 2b/\bar{c}_1(1 - \bar{M}_1^2)$ .

The acoustic waves in the duct downstream of the burning zone are also linear. Neglecting the influence of the entropy fluctuations on the propagation speed and

---

Length of working section upstream of flame zone	$l_u = 1.18$ m
Length of working section downstream of flame zone	$l_b = 0.74$ m
Diameter of duct	$2b = 0.07$ m
Diameter of flame-holder	$2a = 0.035$ m
Flame-holder blockage ratio	25%
Inlet Mach number	$\overline{M}_1 = 0.08$
Inlet stagnation temperature	$\overline{T}_{01} = 293$ K
Equivalence ratio (fuel–air ratio normalized on stoichiometric fuel–air ratio)	$\phi = 0.70$
Fuel	ethylene
Combustion efficiency	0.80

---

TABLE 1. Summary of the geometry and mean flow.

impedance of these waves, we obtain

$$p(x, t) = \overline{p}_2 + h \left( t - \frac{x}{\overline{c}_2 + \overline{u}_2} \right) + j \left( t + \frac{x}{\overline{c}_2 - \overline{u}_2} \right) \quad (3.7a)$$

and

$$u(x, t) = \overline{u}_2 + \frac{1}{\overline{\rho}_2 \overline{c}_2} \left( h \left( t - \frac{x}{\overline{c}_2 + \overline{u}_2} \right) - j \left( t + \frac{x}{\overline{c}_2 - \overline{u}_2} \right) \right) \quad (3.7b)$$

for  $0 \leq x \leq l_b$ . There are also entropy fluctuations in this downstream region which may influence density and temperature in a nonlinear way. That is why we have set out the conservation equations in the form of (3.2) and (3.3), where  $\rho_2$  and  $T_2$  do not appear explicitly. Application of the open end boundary condition,  $p'(l_b, t) = 0$ , shows that

$$j(t) = -h(t - \tau_D), \quad (3.8)$$

where  $\tau_D = 2l_b/\overline{c}_2(1 - \overline{M}_2^2)$ .

Substitution of (3.5)–(3.8) into (3.2) and (3.3) leads to two equations relating  $g(t)$  and  $h(t)$  to  $Q(t)$  and their values at earlier times:

$$\mathbf{X} \begin{pmatrix} g(t) \\ h(t) \end{pmatrix} = \mathbf{Y} \begin{pmatrix} g(t - \tau_U) \\ h(t - \tau_D) \end{pmatrix} + \begin{pmatrix} 0 \\ (Q(t) - \overline{Q})/\pi b^2 \overline{c}_1 \end{pmatrix}, \quad (3.9)$$

where  $\tau_U$  and  $\tau_D$  are the times taken for acoustic waves to travel up and down the regions upstream and downstream of the flame zone respectively.  $\mathbf{X}$  and  $\mathbf{Y}$  are  $2 \times 2$  matrices, with constant coefficients just involving the mean flow. The full forms of  $\mathbf{X}$  and  $\mathbf{Y}$  are given in the Appendix. Equation (3.9) is identical to (2.17) of Dowling (1997). However, in that earlier work  $Q(t)$  was based on experimental data. Now we can determine it from the kinematic flame model of §2.

The time evolution of the flow from specified initial conditions can be determined in a straightforward way. Let us suppose that the wave strengths  $g(t)$  and  $h(t)$  and the flame front position  $\xi(r, t)$  are known up until a time  $t_1$ . Then the flow at the next time step  $t_1 + \Delta t$  can be calculated by first determining the instantaneous rate of heat release at time  $t_1 + \Delta t$  from (2.9) and (3.1). The values of  $g(t_1 + \Delta t)$  and  $h(t_1 + \Delta t)$  then follow from a solution of (3.9). Flow parameters in  $-l_u \leq x \leq 0$  and  $0 \leq x \leq l_b$  can be deduced from (3.5) and (3.7) respectively. In particular, the unsteady velocity

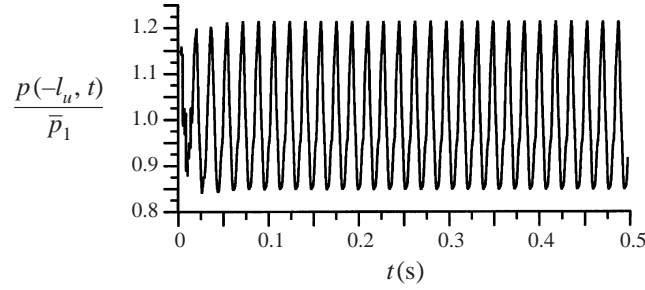


FIGURE 7. Development of limit-cycle oscillations from arbitrary initial conditions for the geometry and flow conditions in table 1.

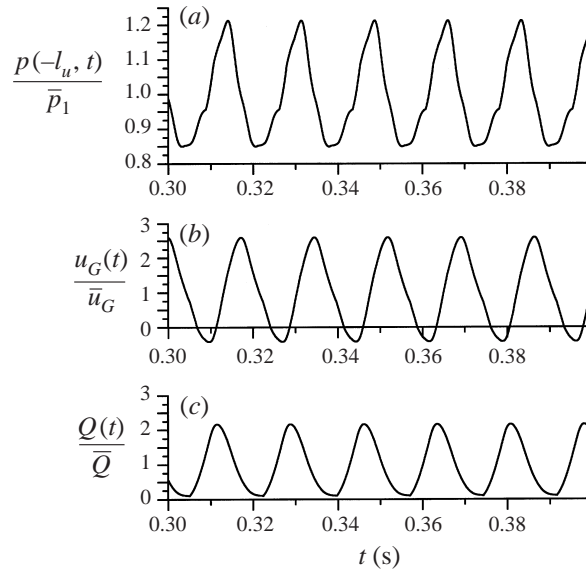


FIGURE 8. Limit-cycle oscillations, conditions as in figure 7: (a)  $p(-l_u, t)$ , (b)  $u_G(t)$ , (c)  $Q(t)$ .

at the flame-holder which influences the flame motion through (2.8) is given by

$$\begin{aligned}
 u_G(t_1 + \Delta t) &= \frac{b^2}{b^2 - a^2} u_1(t_1 + \Delta t) \\
 &= \frac{b^2}{b^2 - a^2} \left( \bar{u}_1 + \frac{1}{\rho_1 \bar{c}_1} \left( -g(t_1 + \Delta t) + \frac{1 - \bar{M}_1}{1 + \bar{M}_1} g(t_1 + \Delta t - \tau_U) \right) \right). \quad (3.10)
 \end{aligned}$$

Finally, the determination of the flow at  $t_1 + \Delta t$  is completed by integration of the flame equation (2.8) with respect to time to determine  $\xi(r, t_1 + \Delta t)$ . In our calculations,  $\xi(r, t)$  was evaluated at 50 locations across the duct radius and a fourth-order Runge–Kutta scheme was used for the numerical time integration.

Figure 7 shows results for the geometry and mean flow summarized in table 1 (Langhorne's 1988, Configuration 1). For this geometry and inlet conditions, we find that linear disturbances are predicted to be unstable at all physically realizable, non-zero fuel–air ratios. To investigate the effects of nonlinearity, the time integration is started from an arbitrary initial condition. A periodic, finite-amplitude oscillation is rapidly established. The fluctuations in pressure, velocity and the rate of heat release in the limit cycle are shown with an expanded timescale in figure 8 and in phase

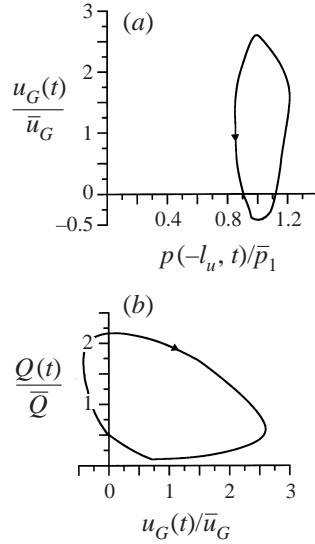


FIGURE 9. Limit-cycle oscillations in phase space, conditions as in figure 7: (a)  $u_G(t)$  vs.  $p(-l_u, t)$ , (b)  $Q(t)$  vs.  $u_G(t)$ .

space in figure 9. There is good agreement with the experimental limit cycles reported by Langhorne (1988). In particular, the flow just reverses during part of the cycle consistent with the observations. There are large-amplitude variations in the rate of heat release, with  $Q(t)$  being nearly zero for part of each cycle, and in agreement with measurement (see Langhorne 1988, figure 11). The limit cycles are also similar to those predicted by Dowling (1997) for the same configuration, using an empirical saturation model for the unsteady heat release. Now we have a more physical basis for the flame model.

We have found that realistic limit cycles for self-sustaining oscillations can be obtained by combining the nonlinear flame model of §2 with linear acoustics and integrating in the time domain. In the next section we investigate how the nonlinear flame model is able to control the limit-cycle amplitude.

#### 4. Describing function analysis

Describing function analysis, as described for example in Ogata (1970), enables us to develop a quasi-nonlinear theory to estimate the limit-cycle amplitude and the frequency of oscillation. This approximate theory has two advantages. First it highlights the physical mechanism by which nonlinearity controls the amplitude of oscillation. Secondly, it enables the analysis of the duct acoustics to be carried out in the frequency rather than the time domain. For the geometry in figure 6, the acoustic waves are reflected in a simple way from the ends of the duct and it is feasible to analyse these waves in the time domain as in §3. However, for more practical combustors, perhaps consisting of multiple supply streams, it is more convenient to analyse the duct acoustics in the frequency domain (see Macquisten & Dowling 1995). Describing function analysis enables us to combine frequency-domain calculations with the nonlinear kinematic flame model.

For disturbances proportional to  $e^{i\omega t}$ , equation (3.9) leads to

$$\underbrace{\left( \mathbf{X} - \mathbf{Y} \begin{pmatrix} e^{-i\omega\tau_U} & 0 \\ 0 & e^{-i\omega\tau_D} \end{pmatrix} \right)}_{\mathbf{M}} \begin{pmatrix} \hat{g}(\omega) \\ \hat{h}(\omega) \end{pmatrix} = \begin{pmatrix} 0 \\ \hat{Q}(\omega)/\pi b^2 \bar{c}_1 \end{pmatrix}, \quad (4.1)$$

where the circumflex denotes a complex amplitude. This can be readily solved to relate  $\hat{g}(\omega)$  and  $\hat{h}(\omega)$  to  $\hat{Q}(\omega)/\pi b^2 \bar{c}_1$ . The velocity fluctuation at the flame-holder  $\hat{u}_G(\omega)$  then follows from (3.10) and we write it in the form

$$\frac{\hat{u}_G(\omega)}{\bar{u}_G} = G(\omega) \frac{\hat{Q}(\omega)}{\bar{Q}} \quad (4.2)$$

with

$$G(\omega) = \frac{\bar{Q} (\mathbf{X}_{12} - \mathbf{Y}_{12} e^{-i\omega\tau_D})}{\pi(b^2 - a^2)\bar{\rho}_1 \bar{u}_G \bar{c}_1^2 \det \mathbf{M}} \left( 1 - \frac{1 - \bar{M}_1}{1 + \bar{M}_1} e^{-i\omega\tau_u} \right). \quad (4.3)$$

The function  $G(\omega)$  calculated in this way is the transfer function between velocity fluctuations at the flame-holder and unsteadiness in the rate of heat release. It essentially accounts for the linear duct acoustics and describes the generation of acoustic waves by unsteady heat input. It depends on the duct geometry, mean flow and sound speed. To complete the solution, the nonlinear kinematic flame model must be used to determine the flame response to  $\hat{u}_G(\omega)$ .

Consider a harmonic variation in the flow velocity at the flame-holder

$$u_G(t) = \bar{u}_G(1 + V \sin \omega t). \quad (4.4)$$

The response of the flame to this imposed velocity fluctuation was investigated in §2. For example, figures 4 and 5 show the periodic motion of the flame and the change in flame surface area  $A(t)$  for particular values of forcing amplitude  $V$  and frequency  $\omega$ . In our model the fluctuations in the rate of heat release are related to the flame area through (3.1):

$$Q(t) = \bar{Q} A(t - \bar{\tau}) / \bar{A}, \quad \bar{\tau} = 0.4l_b / \bar{u}_1. \quad (4.5)$$

For nonlinear forcing of the form in (4.4),  $Q(t)$  is not harmonic but it is still periodic of period  $2\pi/\omega$ .  $Q(t)$  can therefore be expanded as a Fourier series which we write in the form

$$Q(t) = \sum_{-\infty}^{\infty} \hat{Q}_n e^{in\omega t},$$

where

$$\hat{Q}_n = \frac{\omega}{2\pi} \int Q(t) e^{-in\omega t} dt \quad (4.6)$$

and the integral is to be evaluated over one period of oscillation.

In §2.1 we calculated the rate of heat release analytically for linear harmonic velocity oscillations ( $V \ll 1$ ). We note this linear form by a subscript  $L$ . Only  $\hat{Q}_{L0}$ ,  $\hat{Q}_{L1}$  and  $\hat{Q}_{L-1}$  are non-zero.  $\hat{Q}_{L0}$  is of course just  $\bar{Q}$ , the mean value of  $Q(t)$ .  $\hat{Q}_{L1}$  can be calculated from (2.15), (4.5) and (4.6), with the result

$$\frac{\hat{Q}_{L1}}{\bar{Q}} = \frac{\hat{u}_G}{\bar{u}_G} F(\omega) e^{-i\omega\bar{\tau}}, \quad (4.7)$$

where  $F(\omega) = f(\Omega)$ , with  $\Omega = \omega(b - a)/S_u(1 - S_u^2/\bar{u}_G^2)^{1/2}$  and  $f(\Omega)$  is given in (2.18).

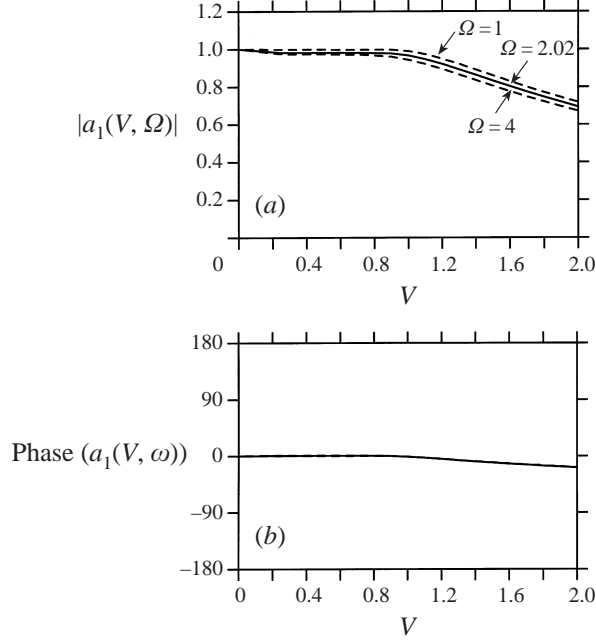


FIGURE 10. The variation of the complex gain  $a_1(V, \omega) = \hat{Q}_L / \hat{Q}_{L1}$  with  $V$ , (a) magnitude, (b) phase, conditions as in figure 7.

For nonlinear fluctuations it is convenient to normalize  $\hat{Q}_1$  on  $\hat{Q}_{L1}$ , the value for linear theory for the same frequency of velocity fluctuations. We introduce a normalized complex gain

$$a_1(V, \omega) = \frac{\hat{Q}_1}{\hat{Q}_{L1}}. \quad (4.8)$$

$a_1(V, \omega)$  may be evaluated by solving numerically for the flame area as in §2.2 and using (4.5) and (4.6) to calculate the first Fourier coefficient. Dividing the resulting  $\hat{Q}_1$  by  $\hat{Q}_{L1}$  from (4.7), with  $\hat{u}_G$  from (4.4), leads to  $a_1(V, \omega)$ . Its magnitude and phase are plotted in figure 10 and we note that they have a particularly simple form. Of course, from its definition we know that  $a_1(V, \omega) = 1$  for small  $V$ . However, from our numerical calculations it emerges that  $a_1(V) \simeq 1$  for all  $V \leq 1$ . We noted from figure 5 that linear theory gives a good approximation to the flame area until flow reversal occurs. The effects of nonlinearity are particularly simple;  $a_1(V, \omega)$  is always effectively real and only has a weak dependence on frequency. For  $V > 1$ ,  $a_1(V, \omega)$  decreases gradually with increasing  $V$ , indicating that the nonlinearity is in the form of a saturation. Once the amplitude of the inlet velocity fluctuations exceeds their mean value, the velocity becomes negative during part of the cycle, the unsteady flame area does not change as much (see figure 5) and the amplitude of perturbation in the rate of heat release is less than predicted from linear theory.

Equations (4.7) and (4.8) lead to

$$\frac{\hat{Q}_1}{\hat{Q}} = \frac{\hat{u}_G}{u_G} a_1(V, \omega) F(\omega) e^{-i\omega\bar{\tau}}. \quad (4.9)$$

This is the essential step in applying describing function analysis: the response in

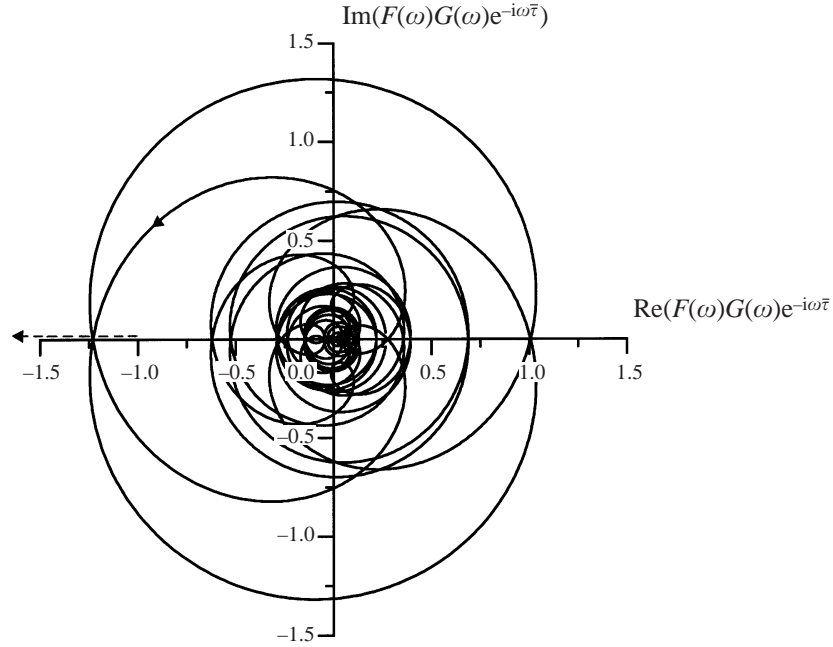


FIGURE 11. Nyquist stability curves: —, locus of  $F(\omega)G(\omega)e^{-i\omega\bar{\tau}}$ ,  $-\infty \leq \omega \leq \infty$ ,  $\omega$  real; -----, locus of  $-[a_1(V, \omega)]^{-1}$ ,  $0 \leq V \leq \infty$ .

heat release rate due to nonlinear velocity fluctuations has been written in terms of the product of the linear response and a gain  $a_1(V, \omega)$ . Combining (4.2) and (4.9), we obtain the characteristic equation for quasi-linear oscillations:

$$\frac{1}{a_1(V, \omega)} + F(\omega)G(\omega)e^{-i\omega\bar{\tau}} = 0. \quad (4.10)$$

Oscillations of magnitude  $\bar{u}_G V$  grow in time, if this equation has any roots with  $\text{Re}(i\omega) > 0$ , whereas, if all the roots have  $\text{Re}(i\omega) < 0$ , the perturbations decrease.

The roots of (4.10) are most conveniently investigated by plotting the Nyquist curve for  $F(\omega)G(\omega)e^{-i\omega\bar{\tau}}$  and the locus of  $-[a_1(V, \omega)]^{-1}$ ,  $0 \leq V \leq \infty$ . These are shown in figure 11 for the geometry and flow conditions in table 1. The Nyquist curve crosses the negative real axis at  $\omega_c = 370 \text{ rad s}^{-1}$ , where  $FGe^{-i\omega\bar{\tau}} = -1.2$ . For small  $V$ ,  $-[a_1(V, \omega)]^{-1} = -1$  which lies to the right of this crossing point. The Nyquist curve therefore encircles  $-[a_1(V, \omega)]^{-1}$ . Since there is then an unstable root, the disturbance grows in magnitude, increasing  $V$  and so (from figure 10) moving  $-[a_1(V, \omega)]^{-1}$  to the left. In a similar way, the Nyquist curve shows that any large-amplitude oscillation with  $-[a_1(V, \omega)]^{-1}$  less than  $-1.2$  is stable and decays in amplitude, moving  $-[a_1(V, \omega)]^{-1}$  to the right. The limit-cycle amplitude is the value of  $V$  for which  $-[a_1(V, \omega_c)]^{-1} = -1.2$ , where  $\omega_c$  is the frequency at which the Nyquist curve crosses the negative real axis;  $\omega_c$  corresponds to a non-dimensional frequency of 2.02, the particular case plotted in figure 10. It follows from figure 10 that  $-[a_1(1.65, \omega_c)]^{-1} = -1.2$ . Any disturbance whose amplitude is less than 1.65 grows, while one whose amplitude  $V$  is greater than 1.65 decays: in the limit cycle we must have  $V = 1.65$ . In other words, the limit-cycle amplitude and frequency of oscillation  $\omega$  are given by the value of  $V$ , which makes  $\omega$ , the root of equation (4.10), real. In this example this corresponds to a peak-to-peak velocity fluctuation of  $3.1\bar{u}_G$  in the

velocity at the flame-holder at a frequency of 58.8 Hz, in excellent agreement with  $3.0\bar{u}_G$  at 57.7 Hz calculated from the full nonlinear theory and shown in figures 8(b) and 9(a).

For this configuration the ducted flame is linearly unstable because the rate of acoustic energy gained from the unsteady combustion exceeds that lost at the duct exit. The energy lost increases in proportion to  $V^2$ , but the energy gain does not grow as rapidly because saturation occurs in the rate of heat release (see figure 10). The limit cycle corresponds to the amplitude  $V$  at which there is an energy balance. Describing function analysis provides a way of determining that amplitude and the frequency of the limit-cycle oscillation from a quasi-linear theory.

## 5. Conclusions

The constant flame speed approach of Fleifil *et al.* (1996) has been extended to model the unsteady behaviour of a ducted flame stabilized in the wake of a bluff centre-body. Of course, such a simplified model does not contain all the details of the flame dynamics. Nevertheless, important large-scale flow features that couple to the duct acoustics are reproduced. For linear harmonic velocity fluctuations, the model has the great advantage that the time variation in the rate of heat release can be calculated analytically. Moreover, this form is in excellent agreement with experimental data. For large-amplitude variations in velocity, the predicted flame front undergoes significant distortion, involving propagation upstream of the flame-holder, reattachment, and ‘necking’ in which an abrupt change occurs in the slope of the flame surface and is subsequently convected downstream. All these features are consistent with previous flow visualizations of the flame.

Self-excited oscillations can be investigated by combining the nonlinear kinematic flame model with linear duct acoustics. In this approach we have treated the heat input as concentrated at a single axial plane. This leads to some inaccuracy in the predicted frequency, but clarifies the role of the nonlinearities. We have concentrated on Langhorne’s (1988) Configuration 1. For that case, the flow is predicted to be unstable at all realistic fuel–air ratios. Weak disturbances grow into limit cycles which reproduce the main experimental observations. Flow reversal is predicted to occur during part of the cycle and the flame moves upstream of the flame-holder. Although the velocity and rate of heat release undergo fluctuations of the order of their mean, the fractional change in the pressure remains small.

Describing function analysis has highlighted the main influence of nonlinearity. Once the flow velocity reverses, the fluctuation in heat release rate ‘saturates’ leading to finite-amplitude limit cycles. Through the introduction of a nonlinear gain which describes this saturation, it is possible to obtain reasonable estimates of the limit-cycle amplitude and frequency from a quasi-linear theory which can be implemented in the frequency domain.

## Appendix

The full forms of the  $2 \times 2$  matrices in equation (3.9) are

$$\mathbf{x} = \begin{pmatrix} -1 + \bar{M}_1 \left( 2 - \frac{\bar{u}_2}{\bar{u}_1} \right) - \bar{M}_1^2 \left( 1 - \frac{\bar{u}_2}{\bar{u}_1} \right) & 1 + \bar{M}_1 \frac{\bar{\rho}_1 \bar{c}_1}{\bar{\rho}_2 \bar{c}_2} \\ \frac{1 - \gamma \bar{M}_1}{\gamma - 1} + \bar{M}_1^2 - \bar{M}_1^2 (1 - \bar{M}_1) \frac{1}{2} \left( \frac{\bar{u}_2^2}{\bar{u}_1^2} - 1 \right) & \frac{\bar{c}_2 (1 + \gamma \bar{M}_2)}{\bar{c}_1 (\gamma - 1)} + \bar{M}_1 \bar{M}_2 \frac{\bar{\rho}_1}{\bar{\rho}_2} \end{pmatrix},$$

$$\mathbf{Y} = \begin{pmatrix} \frac{1 - \bar{M}_1}{1 + \bar{M}_1} \left( 1 + \bar{M}_1 \left( 2 - \frac{\bar{u}_2}{\bar{u}_1} \right) + \bar{M}_1^2 \left( 1 - \frac{\bar{u}_2}{\bar{u}_1} \right) \right) & 1 - \bar{M}_1 \frac{\bar{\rho}_1 \bar{c}_1}{\bar{\rho}_2 \bar{c}_2} \\ \frac{1 - \bar{M}_1}{1 + \bar{M}_1} \left( \frac{1 + \gamma \bar{M}_1}{\gamma - 1} \right. \\ \quad \left. + \bar{M}_1^2 - \bar{M}_1^2 (1 + \bar{M}_1) \frac{1}{2} \left( \frac{\bar{u}_2^2}{\bar{u}_1^2} - 1 \right) \right) & -\frac{\bar{c}_2}{\bar{c}_1} \frac{(1 - \gamma \bar{M}_2)}{\gamma - 1} - \bar{M}_1 \bar{M}_2 \frac{\bar{\rho}_1}{\bar{\rho}_2} \end{pmatrix}.$$

## REFERENCES

- ABU-ORF, G. M. & CANT, R. S. 1996 *Proc. Joint Meeting of Spanish, Portuguese, Swedish & British Sections of Combust. Inst.*
- AHMED, S. A. & NEJAD, A. S. 1992 *Intl. J. Heat Fluid Flow* **13**, 15–21.
- AWAD, E. & CULICK, F. E. C. 1986 *Combust. Sci. Tech.* **46**, 195–222.
- BLOXSIDGE, G. J. 1987 Reheat buzz, an acoustically driven combustion instability, PhD thesis, University of Cambridge.
- BLOXSIDGE, G. J., DOWLING, A. P. & LANGHORNE, P. J. 1988 *J. Fluid Mech.* **193**, 445–473.
- BOYER, L. & QUINARD, J. 1990 *Combust. Flame* **82**, 51–65.
- BROOKES, S. J., CANT, R. S. & DOWLING, A. P. 1999 *ASME 99-GT-112*.
- CATLIN, C. A., FAIRWEATHER, M. & IBRAHIM, S. S. 1995 *Combust. Flame* **102**, 115–128.
- CULICK, F. E. 1988 *AGARD CP 450*.
- CULICK, F. E. C. 1994 *AIAA J.* **32**, 146–169.
- DOWLING, A. P. 1995 *J. Sound Vib.* **180**, 557–581.
- DOWLING, A. P. 1997 *J. Fluid Mech.* **346**, 271–290.
- FLEIFIL, M., ANNASWAMY, A. M., GHONIEM, Z. & GHONIEM, A. F. 1996 *Combust. Flame* **106**, 487–510.
- HEDGE, V. G., REUTER, D. & ZINN, B. T. 1988 *AIAA J.* **26**, 532–537.
- JONES, B. 1974 *Reheat Buzz Film*. Combustion Department, Rolls-Royce Derby.
- KAILASANATH, K., GARDNER, J. H., ORAN, E. S. & BORIS, J. P. 1991 *Combust. Flame* **86**, 115–134.
- KELLER, J. O., VANEVELD, L., KORSCHOLT, D., HUBBARD, G. L., GHONIEM, A. F., DAILY, J. W. & OPPENHEIM, A. K. 1982 *AIAA J.* **20**, 254–262.
- KERSTEIN, A. R., ASHURST, W. T. & WILLIAMS, F. A. 1988 *Phys. Res. A* **37**, 2728–2731.
- LANGHORNE, P. J. 1988 *J. Fluid Mech.* **193**, 417–443.
- LORES, M. E. & ZINN, B. T. 1973 *Combust. Sci. Tech.* **7**, 245–256.
- MACQUISTEN, M. A. & DOWLING, A. P. 1993 *Combust. Flame* **94**, 253–264.
- MACQUISTEN, M. A. & DOWLING, A. P. 1995 *J. Sound Vib.* **188**, 545–560.
- MARGOLIS, S. B. 1993 *J. Fluid Mech.* **253**, 67–103.
- MARKSTEIN, G. H. 1964 *Nonsteady Combustion Propagation*. The Macmillan Company, Pergamon Press, Oxford.
- MENON, S. & JOU, W.-H. 1991 *Combust. Sci. Tech.* **75**, 53–72.
- OGATA, K. 1970 *Modern Control Engineering*. Prentice-Hall.
- OHTSUKA, M., YOSHIDA, S., INAGE, S. & KOBAYASHI, N. 1998 *ASME 98-GT-581*.
- PITZ, R. W. & DAILY, J. W. 1981 *AIAA 19th Aerospace Meeting*.
- POINSOT, T. & CANDEL, S. M. 1988 *Combust. Sci. Tech.* **61**, 121–153.
- POINSOT, T., TROUVÉ, A. C., VEYNANTE, D. P., CANDEL, S. M. & ESPOSITO, E. 1987 *J. Fluid Mech.* **177**, 265–293.
- RAYLEIGH, LORD 1896 *The Theory of Sound*. Macmillan.
- SCHADOW, K. C. & GUTMARK, E. 1992 *Prog. Energy Combust. Sci.* **18**, 117–132.
- SCHADOW, K. C., WILSON, R. J. & GUTMARK, E. 1988 *AIAA J.* **25**, 1164–1170.
- SIVASEGARAM, S., THOMPSON, B. E. & WHITELAW, J. H. 1989 *AIAA J. Propulsion* **5**, 109–115.
- SIVASEGARAM, S. & WHITELAW, J. H. 1987 *Combust. Flame* **68**, 121–130.
- SMART, A. E., JONES, B. & JEWEL, N. T. 1976 *AIAA Paper 76-141*.
- SMITH, D. A. & ZUKOSKI, E. E. 1985 *AIAA Paper 85-1248*.
- STERLING, J. D. & ZUKOSKI, E. E. 1987 *AIAA Paper 87-0220*.

- SUBBAIAH, M. V. 1983 *AIAA J.* **21**, 1557–1564.
- WICKER, J. M., YOON, M. W. & YANG, V. 1995 *J. Sound Vib.* **184**, 141–171.
- YAMAGUCHI, S., OHIWA, N. & HASEGAWA, T. 1985 *Combust. Flame* **62**, 32–41.
- YANG, V. & CULICK, F. E. C. 1986 *Combust. Sci. Tech.* **45**, 1–25.
- YU, K. H., TROUVÉ, A. C. & DAILY, J. W. 1991 *J. Fluid Mech.* **232**, 47–72.